J. Fluid Mech. (1981), *vol.* 113, *pp.* 411-432
Printed in Great Britain

A boundary layer topped by a density interface

By J.-F. PIAT† AND E. J. HOPFINGER

Institut de Mécanique (Laboratoire associé au C.N.R.S.),
Université de Grenoble, France

(Received 31 January 1980 and in revised form 11 May 1981)

A rough-wall turbulent boundary layer which grows into a temperature interface situated at the outer edge is investigated experimentally. Reynolds numbers based on boundary-layer thickness δ range from 4×10^3 to 10^4. Overall Richardson numbers Ri^*, defined in terms of the friction velocity and the boundary-layer thickness, are in the range $0 \leqslant Ri^* \lesssim 80$. Measurements of the mean profiles and of the variances of the velocity fluctuations show that the interface acts in some respects like a moving wall: the velocity profile tends towards a turbulent Couette-type profile and the longitudinal r.m.s. turbulent velocity begins to be amplified at the base of the interfacial layer and reaches a maximum in about the centre. Time-lag correlations of fluctuating quantities taken just above the centre of the interfacial layer have a behaviour characteristic of internal waves, namely a 90° phase lag between vertical velocity and temperature fluctuations. These waves occur as short wave packets and propagate mainly horizontally. On the base of the interface the correlations exhibit the usual symmetric behaviour.

The normalized entrainment velocity u_e/u^* decreases when Ri^* increases but does not follow a power law in Ri^*. This is consistent with momentum balance, which indicates that u_e/u^* also depends on the mean-flow Richardson number $Ri_0 = g\Delta T\delta/TU_0^2$ and on the change in momentum and temperature defect. Momentum balance also shows that, when the undisturbed flow has zero pressure gradient, the boundary layer is expected to separate owing to entrainment when $Ri_0 \simeq 0{\cdot}5$.

1. Introduction

Laboratory studies of mixing across density interfaces have provided a better understanding of the physical processes of thermocline and inversion erosion and have proved useful in developing analytical and numerical models. In these models (for a review see e.g. Niiler & Kraus 1977) the main difficulty arises in connection with the parametrization of the entrainment rate across the interfacial layer. The lack of understanding of the entrainment process in the presence of strong density gradients calls for experimental support, and laboratory and field experiments are complementary. The laboratory experiments most frequently referred to by modellers are the shear experiments by Kato & Phillips (1969) and by Kantha, Phillips & Azad (1977), although it is believed that these results are subject to important secondary effects. These effects are indicative of the difficulty encountered in laboratory experiments in stratified flows. Even in the more tractable problem of turbulent mixing across an interface in zero-mean-shear turbulence (Turner 1968; Linden 1975;

† Present address: Onera, 73500, Modane, France.

Hopfinger & Toly 1976) the results are to some extent open to question, particularly concerning Péclet- and Reynolds-number effects.

Shear experiments are generally more realistic than those without mean shear, because in ocean-thermocline and atmospheric-inversion problems the mean shear is a predominant feature. Also, in these situations the mean flow is non-recirculating, contrary to what is observed in smaller fluid bodies like lakes. Experiments in channels without end walls, of the type carried out by Kato & Phillips (1969) and Kantha *et al.* (1977), are therefore most useful (provided that secondary effects can be reduced or properly accounted for) in understanding fully mixing across thermoclines and inversions. In these experiments, a constant surface stress was imposed on a linearly stratified and a two-layered fluid, respectively, in an annular tank. Global measurements were made, giving the deepening of the mixed layer as a function of time. By definition, this deepening rate is the entrainment velocity which, normalized by the friction velocity, shows a behaviour with overall-Richardson-number dependence (based on the friction velocity) of the form Ri^{*-n}. In the experiments of Kantha *et al.* n is not a constant. Simple energy arguments on the other hand give $n = 1$, whereas mean momentum balance, assuming a quasisteady state, gives $n = \frac{1}{2}$. It has been argued by Price (1979) that side-wall friction plays a dominant role in these annular-tank experiments of small width-to-depth ratio and he showed that the results of Kantha *et al.* agree with $u_e/u^* \propto Ri^{*-\frac{1}{2}}$ after appropriate correction for side-wall friction. However, rotation effects have also been invoked to explain the curious behaviour of these experiments (Armi 1977). Clearly, there is a need for further experiments on shear-driven mixing, where these effects are absent or negligible. In addition, information about the mean-flow and turbulence structure would help in the interpretation of the entrainment results and in understanding better the physical processes of mixing across density interfaces.

The experiments described in this paper were conducted in a wind tunnel. Two streams of equal velocity but different temperatures (hot above cold) were merged downstream from a splitter plate resulting in an initially thin stable temperature interface. The rough-wall boundary layer on the lower wall then grew into the interface. It is a situation similar to that of Kantha *et al.*, with a two-layered fluid, but differs in that in the present study U_0 rather than u^* was kept constant; furthermore, the flow was spatially developing rather than time-dependent, which can lead to boundary-layer separation. The advantages of the present experiment are that unwanted rotation and side-wall effects are absent or negligibly small and that detailed measurements of the flow structure can be made. However, the limited tunnel size imposed relatively low Reynolds numbers ($R_\delta \lesssim 10^4$) and relatively low Richardson numbers ($Ri^* \lesssim 80$). With the Péclet number, defined by the longitudinal r.m.s. turbulent velocity and the integral scale, in the range $75 \lesssim P \lesssim 160$. At these low Péclet numbers the molecular contribution to the heat flux across the interfacial layer can be significant (Crapper & Linden 1974).

Previous investigations of the stably stratified boundary layer considered a stabilizing heat flux at the wall (Arya 1975; Nicholl 1970). In the present study the wall is practically adiabatic and the heat flux is a result of entrainment across the interfacial layer. In both situations a reduction in turbulence level is observed but the mechanisms differ. More closely related experiments are those of Lofquist (1960) and Gartrell (1979). However, in these experiments a mean shear was imposed across

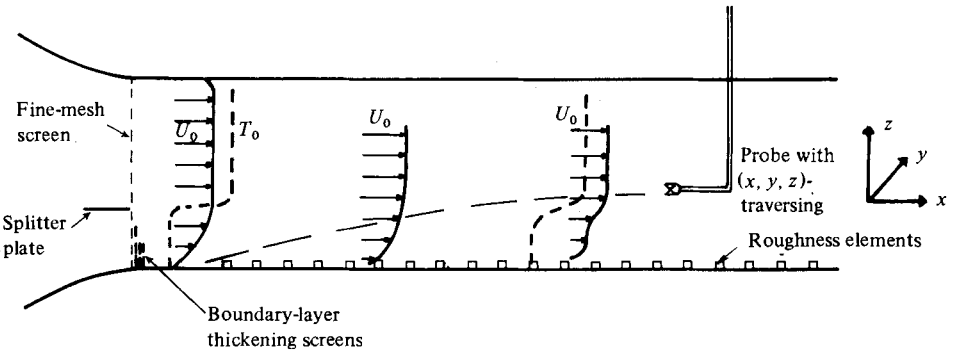

FIGURE 1. Schematic diagram of the wind tunnel.

the interfacial layer and mixing is largely due to shear instability. In the present experiments the shear across the interfacial layer is a result of the inhibition of the downward momentum flux by the temperature interface, and shear production of turbulent kinetic energy in the interfacial layer remains weak.

2. The wind tunnel and working conditions

The experiments were conducted in the wind tunnel shown schematically in figure 1. The test section was 50 cm high, 70 cm wide and 6 m long with an upper wall which could be adjusted for zero axial pressure gradient. At the entrance of the test section two air streams merged past a splitter plate whose wake was practically eliminated by means of a fine-mesh screen placed just downstream. The lower stream was cold, generally at 20 °C, and the upper stream was heated to temperatures between 20° and 60 °C. The temperature interface at the entrance was relatively sharp (< 1 cm thick) and situated 7 cm above the lower wall. The side walls of the tunnel consisted of double walls with electric heating elements sandwiched between.

In order to obtain high Richardson numbers the boundary layer was artificially thickened by means of staggered screens, and the wall was made fully rough. Two-dimensional roughness elements consisting of 8 mm square bars spaced by 9·6 cm were used to give a $z_0 = 0{\cdot}8$ mm and a mean roughness height $k_s = 2{\cdot}7$ cm (Schlichting 1960) at the end of the test section. The ambient velocity U_0 was $50 \lesssim U_0 \lesssim 100$ cm s^{-1} and Reynolds numbers based on δ ranged from 4×10^3 to 10^4. The Richardson number defined as

$$Ri^* = g \frac{\Delta T}{T} \frac{\delta}{u^{*2}},$$

where u^* is the friction velocity, δ the boundary-layer thickness and ΔT the temperature difference between the upper and lower layer, ranged from 0 to about 80.

Measurements were made with two different hot-wire probes, one containing two wires and the other three. The two-wire probe consisted of a DISA gold-plated wire to which a 1 μm 'cold' wire was placed parallel and at 0·8 mm distance. The three-wire probe was made up of a DISA gold-plated X-wire with the 'cold' wire placed perpendicular and slightly off-centre. These probes could be displaced in the (x, y, z)-directions in a continuous manner. Use of the two-wire probe (less subject to errors)

Stability group	Station	U_0 (cm s^{-1})	$\frac{u^*}{U_0}$ (%)	δ (cm)	h (cm)	δ_T (cm)	J	ΔT (°C)	Ri^*	Ri_0	R_δ	P
I	*A*	56·7	5	9·8	3·7	10·4	0·41	20·65	69	0·202	3750	75
	A	52	—	10·5	—	11	—	—	80	—	3770	—
II	*B*	108	5·55	12	4·65	12	0·27	22·1	20	0·070	8650	160
	B	96·4	—	11·6	—	11·6	—	—	23	—	7500	—
III	*B*	108	6·5	13·3	7·2	13·3	0·16	4·9	4·5	0·018	10000	160
IV	*A*	54·3	6·7	12	—	—	—	0	0	0	4500	—
	B	107	6·65	15·4	—	—	—	0	0	0	11000	—

TABLE 1. Boundary-layer parameters for the four stability groups investigated. Station A is 217 cm downstream and station B is 382 cm downstream from the splitter plate.

permitted a check of both the longitudinal fluctuating-velocity component and the longitudinal heat flux.

Calibration was carried out in a special calibration circuit consisting of two jets with nozzle diameters in the ratio 1:2.25. The velocity distribution in the low-speed nozzle was determined with a vortex-shedding probe. Calibration curves were obtained for temperatures between 20° and 55 °C at 5 °C intervals and linear interpolation was used to obtain values at intermediate temperatures. At velocities lower than 50 cm s^{-1}, thermal-wake interaction between the wires was no longer negligible and corrections had to be made. The anemometer signals were passed through signal conditioners, sum and difference circuits, and amplifiers. Their average values were obtained by integrating the analogue signals. Time-lag correlations were carried out using a Schlumberger CNTR 1024 digital correlator. This system has a low cut-off frequency of 0·2 Hz and the sampling frequency in real time is 4 kHz.

The separation of the fluctuating velocity components was accomplished by using operational amplifiers in a manner similar to that described by Schon & Baille (1972). The whole procedure is based on the assumption of small fluctuation levels and is adequate in a boundary layer not too close to the wall. Direct calibration of the wires takes care of the effect of cooling by the axial velocity component which is of increasing importance as the flow speed decreases.

The experimental errors have been estimated to be $\pm 3\%$ for the mean velocity profile, $\pm 5\%$ and $\pm 10\%$ for longitudinal and vertical r.m.s. turbulent velocity respectively, $\pm 10\%$ for longitudinal heat flux and $\pm 15\%$ for Reynolds stress and vertical heat flux. Mean temperatures were measured with $\pm 0{\cdot}1$ °C accuracy.

3. Mean profiles and wall-shear stress

Measurements were made for the four stability conditions listed in table 1. The corresponding Richardson numbers Ri^* are respectively 69 (80), 20 (23), 4·5 and 0, and these are obtained at station A, corresponding to a downstream distance of 217 cm (measured from the end of the splitter plate, figure 1), and station B, corresponding to 382 cm (see table 1). The distance z from the wall is always measured from the middle of the roughness-element height.

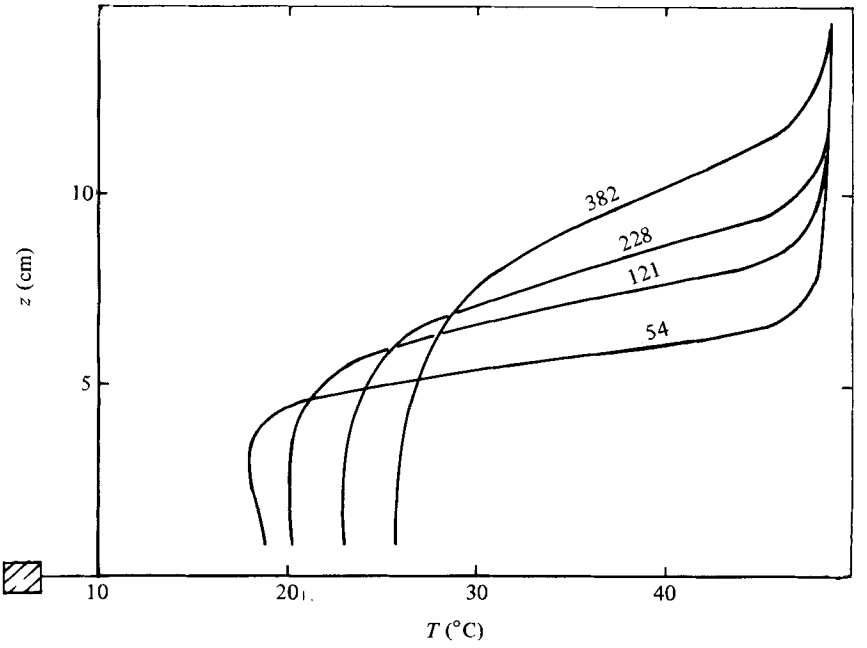

FIGURE 2. Downstream development of temperature profiles for $Ri^* = 20$. The numbers on the curves indicate the downstream distance in cm.

The 'overall' Richardson number Ri^* was defined in §2 and is based on the turbulent boundary-layer thickness δ. This lengthscale, rather than the height of the 'mixed layer', was chosen because it is a better-defined scale and because it corresponds to the definition of Ri^* used by Kato & Phillips (1969) and by Kantha *et al.* (1977) (in their experiments the mixing depth was visualized by using dye). When we refer in the following discussions to the 'mixed layer' we mean the layer in which density gradients are weak, which is the definition used in the oceanographic and meteorological literature (see e.g. Niiler & Kraus 1977).

In addition to δ the thermal-layer thickness δ_T is also used as a length scale. For large Péclet number $\delta_T = \delta$, but for low Péclet number δ_T is somewhat larger than δ (see table 1).

3.1. *Mean profiles*

Figure 2 shows the evolution of the mean temperature distribution for $Ri^* = 23$ at $x = 382$ cm. The mixing across the interface and the resulting heating of the mixed layer are clearly apparent from this figure. The thickness h of the interface defined as $\Delta T/(dT/dz)_{max}$ also increases with downstream distance. Just behind the splitter plate it is about 1 cm thick, at 54 cm it is close to 2 cm, and finally reaches a thickness of 4·65 cm at station B. For higher Richardson numbers ($Ri^* = 80$) the interface evolves in a way similar to that shown in figure 2, whereas for nearly neutral conditions the interface at station B is considerably thicker (table 1); as is expected, because in neutral conditions scalar gradients tend to be smoothed, whereas in highly stable conditions gradients are enhanced.

Since the boundary layer was artificially thickened at the entrance of the test section, it was necessary to investigate the similarity in velocity profiles. Figure 3

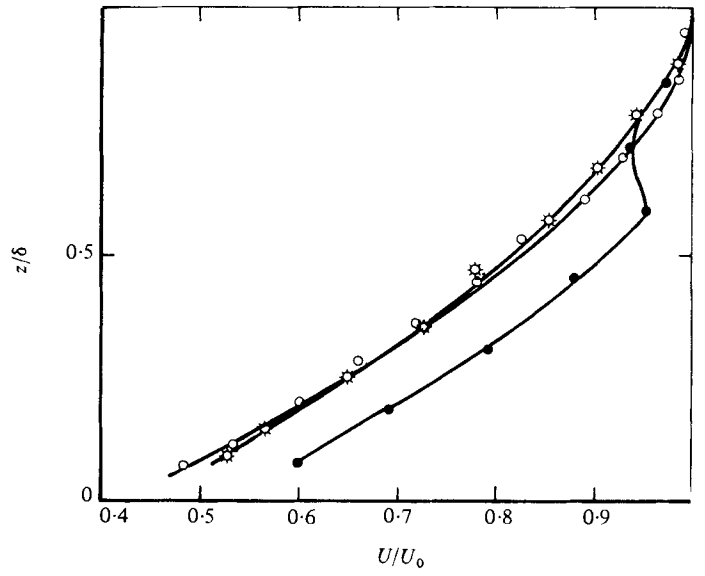

FIGURE 3. Downstream development of velocity profiles for neutral conditions. $U_0 = 54{\cdot}3$ cm s^{-1} ●, $x = 64$ cm, $\delta = 7{\cdot}5$ cm; ☼, $x = 141$ cm; $\delta = 9{\cdot}4$ cm; ○, $x = 217$ cm, $\delta = 12$ cm.

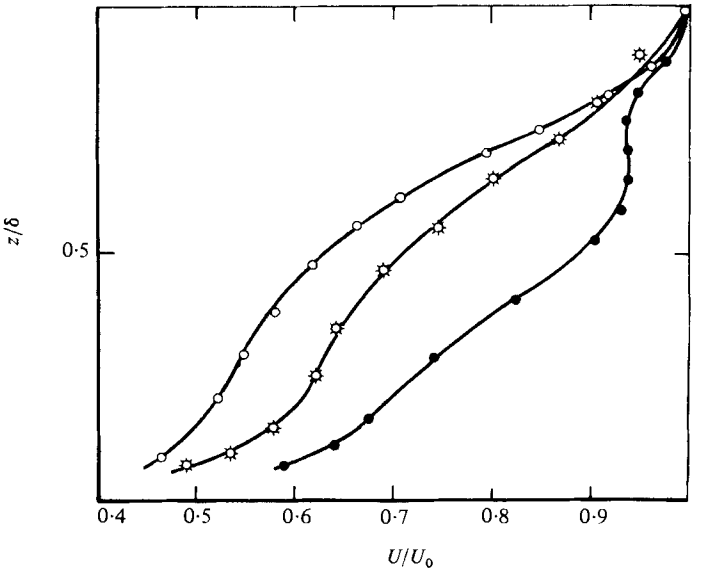

FIGURE 4. Downstream development of velocity profiles for stability group I ($Ri^* = 80$ at station A). The ambient velocity is $U_0 = 52$ cm s^{-1}; ●, $x = 64$ cm, $\delta = 7{\cdot}3$ cm; ☼, $x = 141$ cm, $\delta = 8{\cdot}4$ cm; ○, $x = 217$ cm, $\delta = 10{\cdot}5$ cm.

shows the profiles at $x = 64, 141$ and 217 cm, with $U_0 = 54{\cdot}3$ cm s^{-1} for neutral conditions. Figure 4 shows the corresponding profiles for $Ri^* = 80$. The profiles for the other conditions investigated are similar in behaviour. It is seen that the effect of the thickening screens is still clearly visible at 64 cm, but beyond 120 cm the profiles show a similarity behaviour in the neutral case (figure 3). When an interface is present the velocity profiles continue to change with downstream distance and this

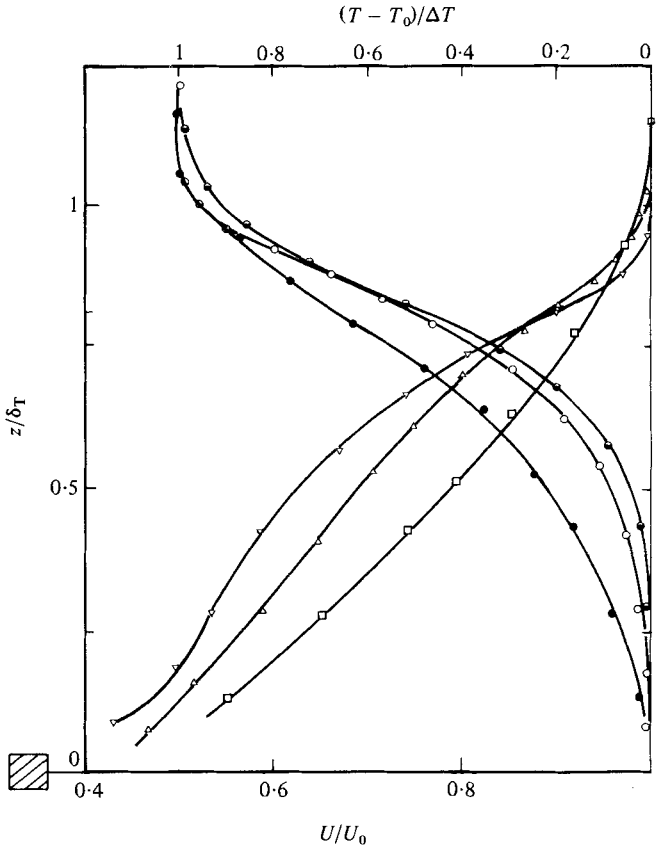

FIGURE 5. Mean velocity and temperature profiles at stations A and B for stability groups I, II and III. Group I: $Ri^* = 69$; ▽, velocity; ◒, temperature. Group II: $Ri^* = 20$; △, velocity; ○, temperature. Group III: $Ri^* = 4$, 5; □, velocity; ●, temperature. See table 1 for corresponding values of U_0, ΔT, δ and δ_T.

change is much more marked when Ri^* is high. A clear decrease in growth rate is also observed. This evolution does not depend on the initial velocity profile, as was verified experimentally by imposing an intentional mismatch in the velocity of the lower and upper streams at the test-section inlet. The evolution is partly due to the fact that Ri^* increases with downstream distance. It is assumed that the profiles measured at stations A and B are in quasi-equilibrium: the turnover time of the turbulent eddies is a small fraction of travel time between the inlet and station A or B.

At stations A and B, where detailed measurements were made for $Ri^* = 20$ and 69, respectively, the two-dimensional nature of the flow was verified. Measurements of mean and turbulent quantities made about one boundary-layer thickness off centre showed similar profiles (Piat 1979). At downstream distances beyond stations A and B this spanwise invariance was no longer observed because side-wall convection started to contaminate the central region.

3.2. *Stability conditions in the interface*

Figure 5 shows that the shear in the interface increases with Ri^* and it is possible that production of turbulent kinetic energy in the interface will occur. The temperature gradient in the interface has a stabilizing effect, however, and, when the interfacial Richardson number

$$J = \frac{g}{T}\frac{\partial T/\partial z}{(\partial U/\partial z)^2}$$

exceeds some critical value J_c, the interface is expected to remain stable. Turbulence coming from below erodes the interface and has a tendency to thin it. Because of this erosion it is possible that J may transiently fall below J_c, resulting in instability and production of turbulence. This production enhances mixing, and consequently a thickening of the interface occurs until the critical value of J is again reached. This process goes on and sporadic interfacial production can occur in a way pointed out by Kantha *et al.* (1977). It is therefore of interest to calculate J from the profiles given in figure 5. The values of J for the three stability conditions investigated are given in table 1. The gradients were taken in the middle of the interfacial layer and correspond closely to the maximum values. In the more stable situations, when a noticeable shear is generated across the interfacial layer, the values of J indicate that the equivalent laminar flow would be stable. The measured values (see table 1) are comparable to the value of about $\frac{1}{3}$ found for relaminarization of a turbulent shear layer (Koop & Browand 1979) although the present situation differs from the mixing-layer configuration by the presence of the adjacent turbulent boundary layer. A closely related problem is the stratified turbulent wall jet in which case the free-mixing zone also ceases to be dynamically active when J reaches a value of about $\frac{1}{3}$ (Hopfinger 1973).

If it is assumed that the thickness of the interfacial layer is set by stability associated with $J = \frac{1}{3}$, then it is possible to get an expression for the relative interfacial layer thickness h/δ as a function of Ri^* in the form

$$\frac{h}{\delta} = \frac{k^2}{3Ri^*},$$

where

$$k = \frac{h}{u^*}(dU/dz)_{\max}.$$

For $Ri^* = 69$ the value of k is about 9, giving $h/\delta = 0{\cdot}39$, which is consistent with the value determined from table 1. The above relation should remain valid for larger Ri^* but it should be noted that the value of k depends on the velocity defect, which is more pronounced at higher Ri^*.

3.3. *Wall-shear stress*

The friction velocity u^* has been obtained in two ways: (i) from direct measurements of Reynolds stresses near the wall, (ii) from momentum integrals between two stations (121 and 382 cm, and 64 and 217 cm). The use of a logarithmic plot proved to be too inaccurate at these low Reynolds numbers. The momentum-integral method gave an averaged value of u^* which was about 5 % higher than u^* obtained from

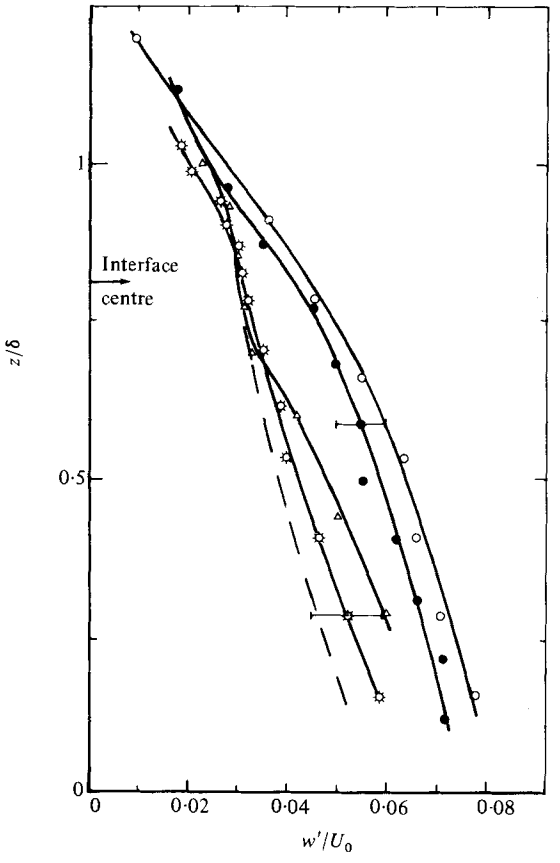

FIGURE 6. Vertical r.m.s. turbulent velocity normalized on free-stream velocity as a function of normalized distance z/δ. ○, $Ri^* = 0$, $R_\delta = 4500$; ●, $Ri^* = 0$, $R_\delta = 10{\cdot}000$; ☼, $Ri^* = 20$, $R_\delta = 8659$; △, $Ri^* = 69$, $R_\delta = 3750$. – – – – expected variation of w' for $Ri^* = 69$, consistent with the friction velocity.

local measurements. The value given in table 1 is the mean of the values obtained by the two methods.

The results show a decrease in u^*/U_0 with increasing Ri^*. This decrease can be attributed entirely to the evolution of the velocity profile from a boundary-layer shape to a profile with more momentum defect (see figure 5). The stratification of the interfacial layer inhibits momentum transfer from the non-turbulent layer to the boundary layer and this effect is felt throughout the boundary layer. The boundary layer adjusts to the reduced downward momentum flux at its outer edge by producing a significant velocity gradient across the interfacial layer (now a region of high resistance) and at the same time reducing the mean gradient in the mixed layer. If, in place of the interfacial layer, the boundary layer were suddenly topped by a wall moving at U_0 a similar evolution of the mean profile would be observed. The limiting state in this case would be the plane-turbulent Couette flow and it is therefore of interest to discuss the observed reduction in u^*/U_0 with reference to the turbulent Couette flow.

In a turbulent boundary layer along a smooth wall the value of $u^*/U_0 = 4 \times 10^{-2}$

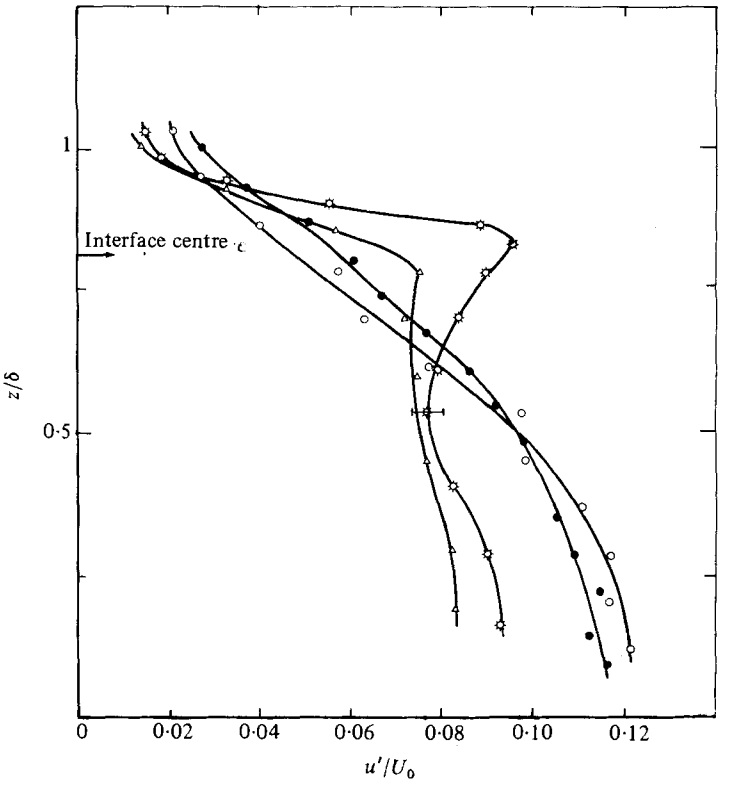

FIGURE 7. Longitudinal r.m.s. turbulent velocity normalized on free-stream velocity as a function of normalized distance z/δ. Symbols ○, ●, ☼, △ refer to same conditions as in figure 6.

for $R_\delta = 10^4$ (Hinze 1975). In a plane Couette flow at the same Reynolds number $u^*/U_0 = 2{\cdot}4 \times 10^{-2}$, or $4{\cdot}8 \times 10^{-2}$ when u^* is referred to the centre velocity as is usual (Robertson & Johnson 1970). The measured rough-wall boundary-layer value is $u^*/U_0 = 6{\cdot}7 \times 10^{-2}$. Unfortunately, no results are available for a fully-rough-wall Couette flow, but it seems reasonable to assume that with a rough wall the Couette friction velocity would also be about 60% of the equivalent rough-wall boundary-layer value. This reasoning gives a value of 4×10^{-2}, and the measured value of 5×10^{-2} for $Ri^* \simeq 80$ lies well within the expected range. It should be noted, however, that at very high values of Ri^* the interface-topped boundary layer could reach values of u^*/U_0 less than the Couette flow limit because of an adverse-pressure-gradient effect due to entrainment (see §5).

In the flat-plate boundary layer investigated by Arya (1975) which was stably stratified by cooling of the floor, u^*/U_0 also decreased with increasing stability. In this case, buoyancy is most effective in the wall region, inhibiting the vertical turbulent motions there, whereas in the interface-topped boundary layer the wall region is affected only through a change in mean velocity profile. As a consequence, the final mean-flow structures differ considerably in the two situations.

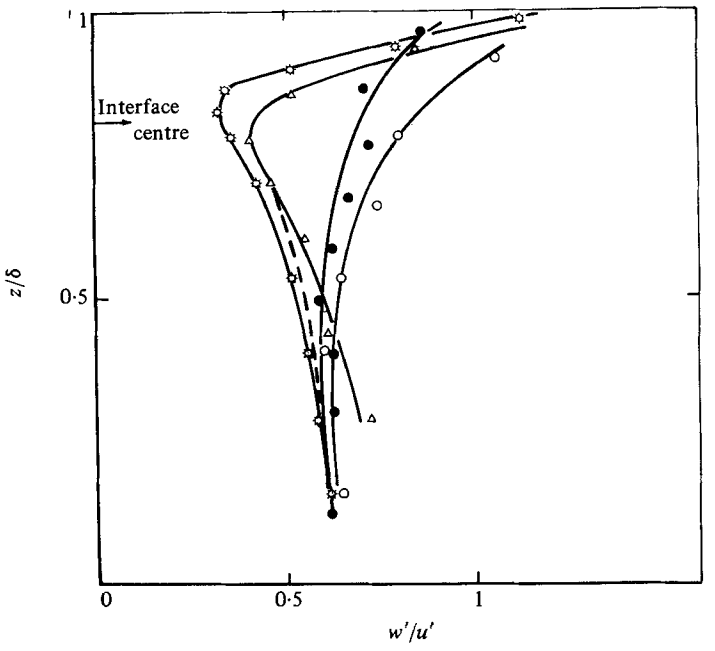

FIGURE 8. Square root of normal-stress ratio w'/u' as a function of normalized distance z/δ. Symbols ○, ●, ☼, △ refer to same conditions as in figure 6. – – – – – expected ratio for $Ri^* = 69$.

4. Turbulence quantities

4.1. *Turbulent velocities*

Figures 6 and 7 show the variation of the vertical and longitudinal r.m.s. turbulent velocities w' and u', normalized by the ambient velocity, as a function of distance from the boundary. When $Ri^* = 4{\cdot}5$ the behaviour does not differ from the neutral case. As seen from table 1, the lower-Reynolds-number neutral flow has a higher value of u^*; this explains the higher values of the r.m.s. turbulent velocities for lower values of R_δ. The reason for the higher u^* is a more effective roughness at station A. When the stability increases, the r.m.s. turbulent velocities in the mixed layer decrease, a result which is essentially a consequence of the decreasing shear production due to the change in the mean velocity profile discussed in §3. The measured vertical r.m.s. turbulent velocity w' in the mixed layer (figure 6) is higher for $Ri^* = 69$ than for $Ri^* = 20$, a result which is contrary to expectations and which seems to have no explanation other than experimental error.† In the wall region w' should scale on the shear velocity u^*, which is lower for $Ri^* = 69$ than for $Ri^* = 20$. The value of w' which would be consistent with u^* is indicated by a dashed line in figure 6. The longitudinal r.m.s. turbulent velocity u' (figure 7) shows a consistent behaviour. This component was measured with straight wires and the experimental error is consequently smaller. In the interfacial layer the turbulent structure is strongly affected by stratification. It is seen from figure 7 that u' reaches a maximum just above the centre of the interfacial layer when $Ri^* = 20$ and then falls off rapidly

† In these runs the mean velocity in the mixed layer is quite small ($\lesssim 30$ cm s^{-1}), which makes hot-wire measurements difficult (corrections for thermal-wake interaction between wires are necessary) and in this case the errors are likely to exceed the estimations given in §2.

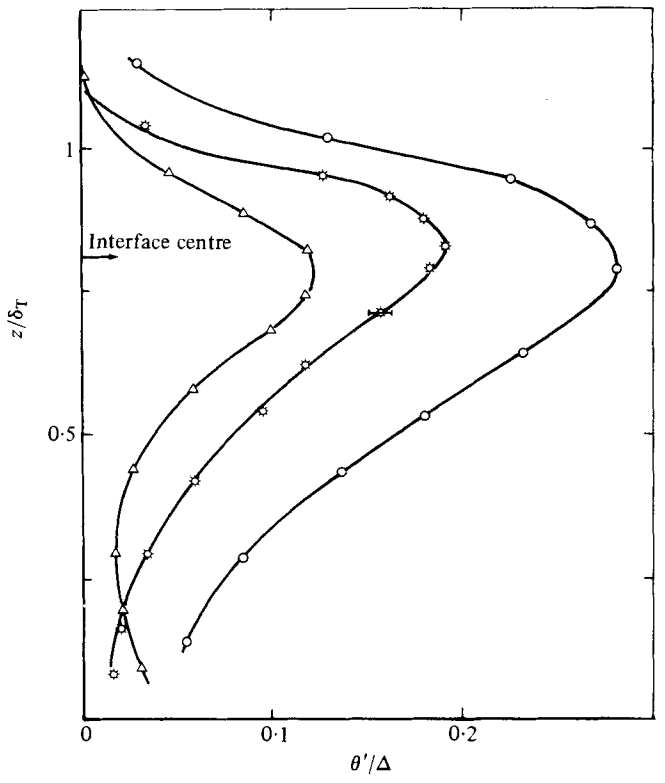

FIGURE 9. Intensity of temperature fluctuations as a function of normalized distance z/δ_T. ○, $Ri^* = 4{\cdot}5$, $P = 160$; ☼, $Ri^* = 20$, $P = 160$; △, $Ri^* = 69$, $P = 75$.

towards the outer edge of the layer. For higher stability ($Ri^* = 69$), on the other hand, u' remains more nearly constant up to the middle of the interfacial layer and then falls off in a similar way.

The vertical r.m.s. velocity shows a nearly uniformly decreasing behaviour over the whole layer, with some indication of a slight hump just above the centre of the interfacial layer. This observation is discussed in §4.4 in the context of internal wave motion.

The relatively larger increase in u' is clearly seen from figure 8, where w'/u' is plotted as a function of distance from the wall. While in the neutral boundary layer the normal stress ratio increases steadily towards the outer edge, in the presence of an interface a sharp drop is observed in the interfacial-layer region. In the mixed layer, where the density gradient is negligible, the neutral value is approached regardless of stability. The dashed line again indicates the value of w'/u' for $Ri^* = 69$, calculated with w', which would be more consistent with the wall-shear stress.

The amplification of u' in the interfacial layer bears a striking similarity to the case of homogeneous turbulence near a rigid surface (Thomas & Hancock 1977). In these experiments the turbulent eddies are flattened as they approach the rigid surface and this leads to an increase in u' relative to w'. Rapid-distortion theory describes this phenomenon and also gives a Reynolds-number criterion for amplifi-

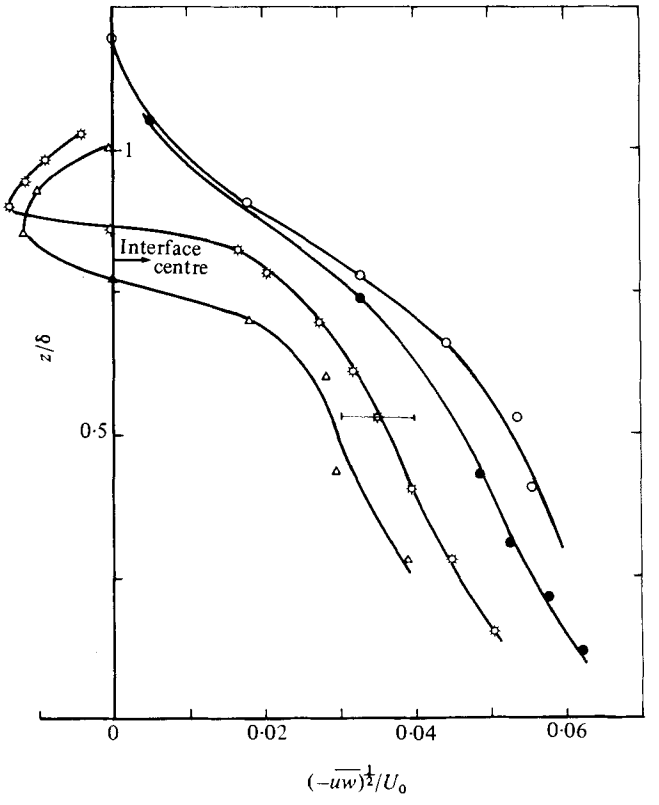

FIGURE 10. Square root of Reynolds stress normalized on U_0 as a function of normalized distance z/δ. The symbols ○, ●, ☼, △ refer to the same conditions as in figure 6.

cation (Hunt & Graham 1978). The condition for amplification is that the integral scale of the unaffected turbulence is $l \gtrsim 5\delta^{\nu}$, where δ^{ν} is a viscous-layer thickness which depends on Reynolds number. For the case $Ri^* = 69$, the Reynolds number $R_l = u'l/\nu = 100$, is close to the value of Uzkan & Reynolds' (1967) free-shear turbulent boundary layer. No amplification was observed by these authors. According to Hunt & Graham, a value of $R_l \simeq 400$ would be required for amplification to occur in free-shear turbulence. We already observe an increase in u' when $R_l = 230$ (the value corresponding to the conditions of $Ri^* = 20$). In view of the difference in flow situations and the uncertainties in the evaluation of δ^{ν} when the distortion is caused by an interfacial layer, we can only conclude that the behaviour is qualitatively similar and that rapid distortion is a plausible explanation for the observed increase in u'.

In principle, it would seem possible that the increase in u' is caused by an increase in production of turbulent kinetic energy in the interfacial layer. Since stratification inhibits the transfer of energy to the w-component, a higher degree of anisotropy is plausible in the interfacial layer. However, an evaluation of the terms $\overline{uw}\,\partial U/\partial z$ and $(u^2-w^2)\,\partial U/\partial z$ shows that, in the mean, production remains weak in spite of the increase in mean strain in the interfacial layer. This argument then implies that the turbulent kinetic energy in the interfacial layer cannot increase by any noticeable amount, and consequently the spanwise component of the r.m.s. velocity should

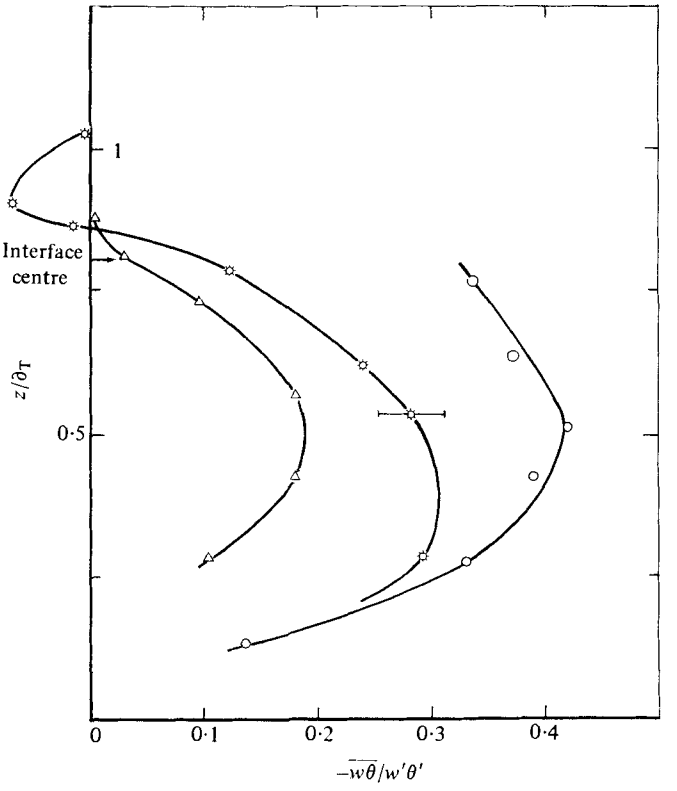

FIGURE 11. Vertical heat-flux correlation coefficient $\overline{w\theta}/w'\theta'$ as a function of normalized distance from the wall z/δ_T. The symbols ○, ☼, △ refer to $Ri^* = 4{\cdot}5$, 20 and 69, as in figure 9.

exhibit no amplification. We have, unfortunately, no results concerning the spanwise r.m.s. velocity to verify this conjecture.

4.2. *Temperature fluctuations*

The r.m.s. value of the temperature fluctuation θ' normalized by the temperature difference ΔT between the mixed layer and the non-turbulent stream is plotted as a function of distance from the wall in figure 9. It is seen that $\theta'/\Delta T$ decreases from a maximum value of close to 0·3 in near-neutral conditions ($Ri^* = 4{\cdot}5$) to a value of 0·2 when $Ri^* = 20$. This decrease in the level of $\theta'/\Delta T$ can be explained by a reduction, due to stratification, in the vertical lengthscale of the turbulent motions. For higher stability the value of $\theta'/\Delta T$ decreases to about 0·11. This low value is believed to be a consequence of low Péclet number ($P = u'l/\kappa = 160$ when $Ri^* = 20$, and 75 when $Ri^* = 69$; here l is the longitudinal integral scale and κ the thermal diffusivity). The results of Crapper & Linden (1974) indicate a marked Péclet-number effect when $P < 200$. The explanation is the existence of a diffusive layer (diffusive core in Crapper & Linden's situation) in the upper part of the interface when P is low; the turbulent motions do not then span the whole interfacial layer. Our values of $\theta'/\Delta T$ are generally about twice the values obtained by Crapper & Linden (for example their maximum value for $P = 155$ and $Ri = 75$ is 0·05). This difference can be ascribed to the fact that turbulence in their experiment was generated on both

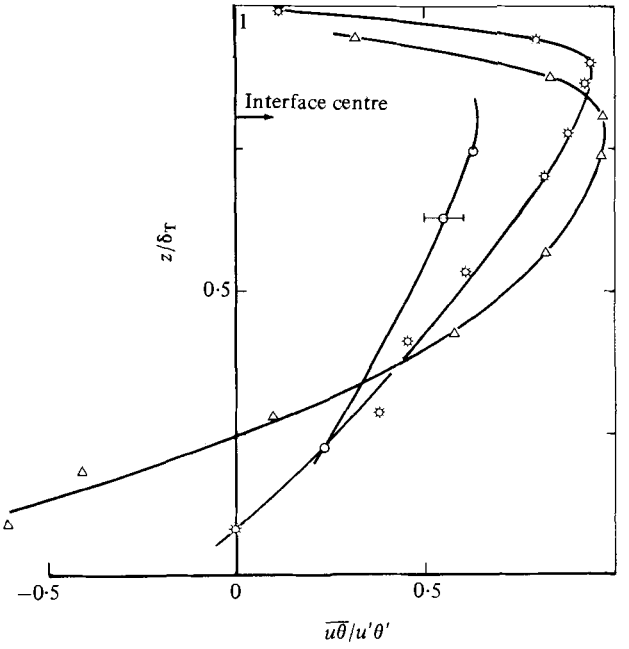

FIGURE 12. Longitudinal heat-flux correlation coefficient $\overline{u\theta}/u'\theta'$ as a function of normalized distance from the wall z/δ_T. The symbols ○, ☼, △ refer to the same conditions as in figure 9.

sides of the interface and for $P < 200$ the eddies penetrated less than half the interfacial layer (presence of a diffusive core).

4.3. *Reynolds stresses and heat-flux variations*

From Reynolds-stress measurements near the wall, values of the friction velocity given in table 1 were obtained and, as mentioned before, these were about 5 % lower than the value calculated from momentum-integral considerations. Figure 10 presents the variation with height of the normalized Reynolds stress for all stability conditions investigated. The Reynolds stress decreases with increasing stability as a result of the reduction in downward momentum transfer discussed in §3.3. Below the interfacial layer the variation is the same as in the neutral boundary layer, but in the interfacial region the Reynolds stress falls rapidly to zero. Weak positive values have been consistently measured in the upper portion of the interfacial layer (see §4.4).

The heat-flux correlations $\overline{w\theta}/w'\theta'$ and $\overline{u\theta}/u'\theta'$ are shown in figures 11 and 12. At the bottom of the boundary layer a change in sign occurs because the wall is slightly heated by radiation. These fluxes are weak and thus have no direct dynamical effects. The figures show clearly that u and θ tend to be better correlated as stability increases. The value of $\overline{u\theta}/u'\theta'$ is close to unity just above the centre of the interfacial layer. In contrast, $\overline{w\theta}$ goes to zero there. Figures 11 and 12 also indicate that the ratio of longitudinal to vertical heat fluxes increases from the neutral value of about 2·5 to very high values in the interface. The observed reversal in sign of $\overline{w\theta}$ just above the middle of the interfacial layer for $Ri^* = 20$ is not sufficiently significant to be dwelt upon. It is largely compensated by molecular effects, as is seen from figure 13, where the total vertical heat flux and the molecular flux are plotted as

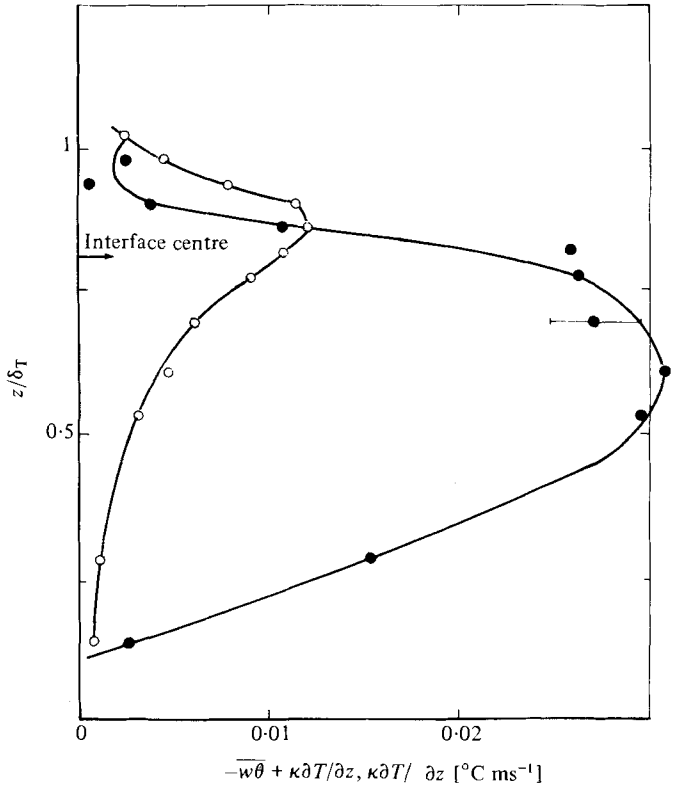

FIGURE 13. Total and molecular vertical heat flux as a function of normalized distance z/δ_T, plotted for stability $Ri^* = 20$, $P = 160$. ●, total; ○, molecular.

functions of z/δ_T for $Ri^* = 20$. For $Ri^* = 69$ a heat-flux curve similar to that of figure 13 is obtained, but with the molecular-flux contribution considerably increased.

The flux Richardson numbers

$$Rf = \frac{g}{T}\frac{\overline{w\theta}}{\overline{uw}\,\partial U/\partial z}, \quad Rs = \frac{g}{T}\frac{\overline{u\theta}}{\overline{w^2}\,\partial U/\partial z}$$

give an indication of the fraction of kinetic energy and Reynolds-stress production which is lost to buoyancy. These two Richardson numbers are shown in figure 14. Values of Rf and Rs have only been calculated up to the centre of the interface, since above it the error, particularly in Rf, would increase considerably as both $\overline{uw}$ and $\overline{w\theta}$ approach zero. In a quasi-equilibrium state the value of Rf as defined above should be < 1 (because of viscous dissipation) when diffusion terms are negligible. The values cited in the literature range from very small values to about 0·3 and the values of Rf shown in figure 14 lie generally within this range. This does not indicate, however, that diffusion is negligible. In fact, as was mentioned in §4.1, production in the interfacial layer remains weak and kinetic energy diffusion from the mixed layer is preponderant. It would be more appropriate in this case to include the diffusion terms in the definition of the flux Richardson number, that is

$$Rf = g\frac{\overline{w\theta}}{T}\Big/\left[\overline{wu}\frac{\partial U}{\partial z} + \frac{\partial}{\partial z}\left(\tfrac{1}{2}q^2\overline{w} + \frac{1}{\rho}\overline{pw}\right)\right].$$

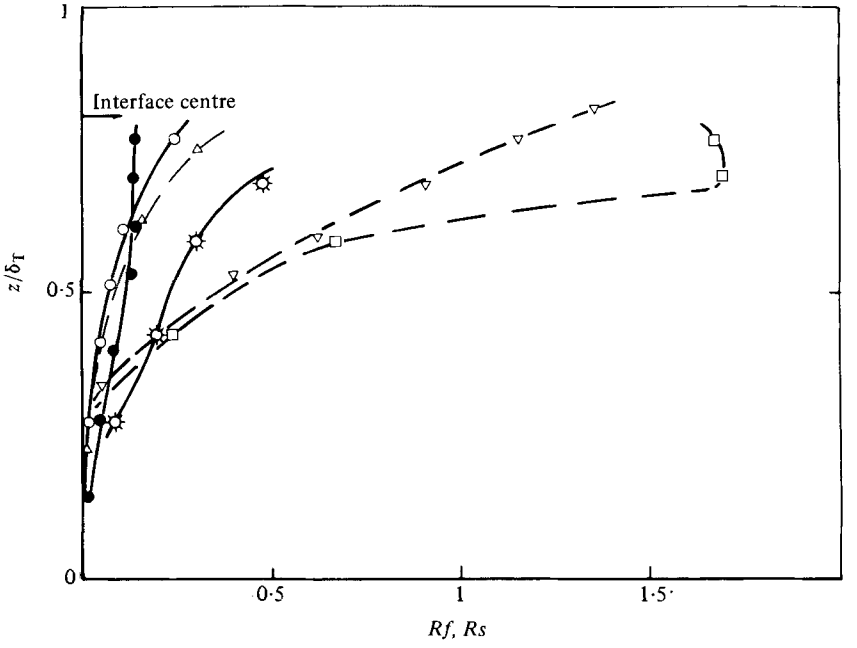

FIGURE 14. Flux Richardson numbers *Rf*, *Rs* plotted as functions of normalized distance from the wall. ☼, *Rf*, □, *Rs* for $Ri^* = 69$; ●, *Rf*, ▽ *Rs* for $Ri^* = 20$; ○, *Rf*, △, *Rs* for $Ri^* = 4{\cdot}5$.

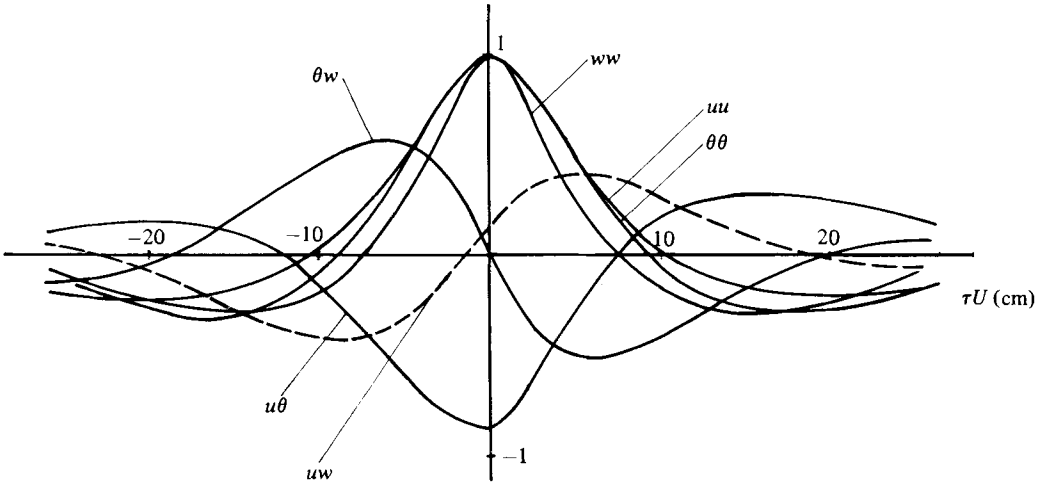

FIGURE 15. Time-lag correlation coefficients $\overline{uu(\tau)}/u'^2$, $\overline{ww(\tau)}/w'^2$, $\overline{\theta\theta(\tau)}/\theta'^2$, $\overline{\theta w(\tau)}/\theta' w'$, $\overline{\theta u(\tau)}/\theta' u'$, $\overline{wu(\tau)}/w' u'$ as functions of the product of time delay τ multiplied by the mean velocity $U = 51{\cdot}3$ cm s^{-1}, taken at $z/\delta_T = 0{\cdot}83$ for $Ri^* = 69$.

Gartrell (1979) found that in stratified flows diffusion of kinetic energy can exceed production.

The values of *Rs* are seen to be much greater than those of *Rf*, which is qualitatively in agreement with the results obtained by Arya (1975) in the stably stratified boundary layer. Since viscous dissipation of Reynolds stresses is negligible, a value of 1 for *Rs* is physically plausible. The measured values of *Rs* shown in figure 14 for

$Ri^* = 20$ and 69, however, reach a value > 1 in about the centre of the interfacial layer. Diffusion of Reynolds stress can explain this observation. Again, if the diffusion terms were included in the definition of Rs the upper limit should not exceed 1.

4.4. *Time-lag correlations*

Figure 15 shows time-lag correlations taken just above the centre of the interfacial layer ($z/\delta_T = 0{\cdot}83$) for stability condition $Ri^* = 69$. It is seen that $\overline{w\theta(\tau)}$ and $\overline{wu(\tau)}$ are odd functions of τ, whereas all other functions are even. The zero value of $\overline{w\theta(0)}$ and the slightly positive value of the Reynolds stress shown on figures 10 and 11 are again brought out by figure 15. When $Ri^* = 20$ a quite similar picture is obtained, but the position where $\overline{wu(0)} = 0$ is situated closer to the upper edge of the interfacial layer. In the mixed layer all functions are symmetric for all stability groups, as would be expected.

The observed 90° phase shift between the vertical-velocity fluctuations and the scalar-field fluctuations is characteristic of internal wave motion. Wave motion also gives rise to a nearly 90° phase shift between w and u, and in the presence of a mean shear a transfer of wave energy to the mean field can occur (Phillips 1966, p. 178). This is probably the reason for the measured weak positive values of $\overline{wu(0)}$. Wave motion has also been mentioned as a possible explanation of the relative increase in u' (McDougall 1979). Nearly vertically propagating internal waves would indeed have a large value of u'. For this reason it is of interest to know the type of waves which are predominant.

The waves are excited by the turbulent eddies impinging on the interfacial layer in a way similar to the impingement of a vortex ring investigated by Linden (1973). Their integral scale is $l \simeq 4$ cm (obtained from autocorrelation in the mixed layer), and their recoil time is $\tau = (l/g)^{\frac{1}{2}} (\Delta T/T)^{-\frac{1}{2}} = 0{\cdot}25$ s. Since these eddies are convected past the probe at $U \simeq 50$ cm s^{-1} (conditions corresponding to figure 15), the half-wavelength $\frac{1}{2}\lambda = U\tau = 12{\cdot}5$ cm. This wavelength corresponds closely to the measured value (figure 15), which indicates that the dominant waves are horizontally propagating interfacial waves. The slight hump in w' observed in the interfacial layer (figure 6) could be attributed to these waves, but the relative increase in u' cannot be explained by wave motion of the type exhibited by the time-lag cross-correlations. Figure 15 also shows that the waves occur as short wave packets. This is to be expected, since the interfacial layer is continuously forced by randomly impinging eddies.

5. Entrainment rate and momentum balance

5.1. *Entrainment velocity*

The entrainment rate can be determined from the spatial growth of the boundary-layer thickness. The entrainment velocity is just given by $u_e = (d\delta/dx)\, U_0$ and, in principle, it seems an easy task to determine u_e. However, the relatively small growth rate can cause large errors in the determination of $d\delta/dx$ and, in order to obtain u_e with reasonable accuracy, the change in height over the largest possible distance was taken. When $U_0 = 100$ cm s^{-1}, we determined $\Delta\delta$ between $x = 121$ and 382 cm and when $U_0 = 50$ cm s^{-1} between $x = 64$ and 217 cm. The value of Ri^* varied somewhat

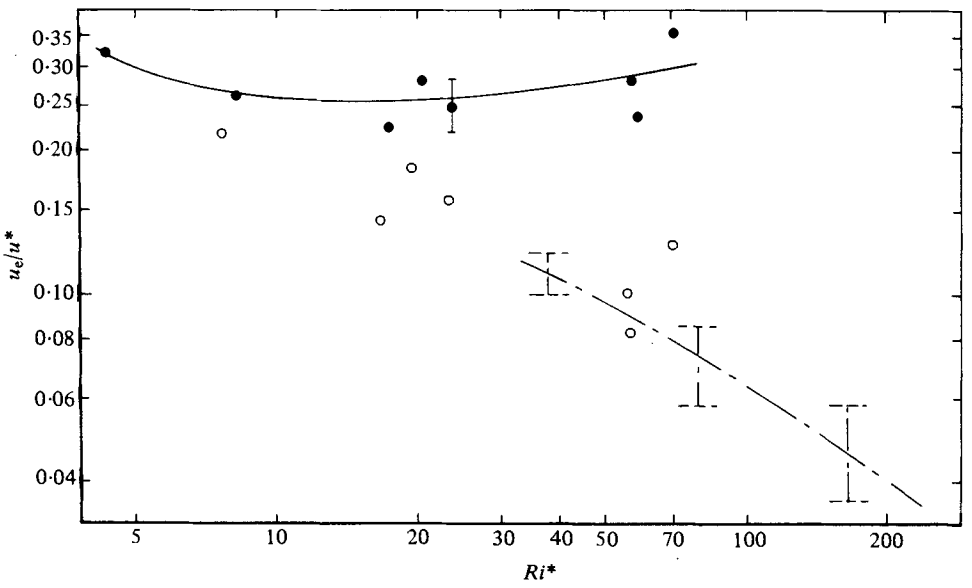

FIGURE 16. Normalized entrainment velocity plotted logarithmically as a function of Ri^*. ●, observed values; ○, values corrected for molecular flux; ———, results of Kantha *et al.* (1977).

between the two stations (for instance from 14·3 to 20 when $U_0 = 100$ cm s^{-1}) and the mean value was used for correlating the entrainment velocity shown in figure 16. It is seen from this figure that u_e/u^* varies very little with Ri^* in the range of Ri^* studied. It is, however, important to note that u_e does decrease with increasing Ri^* but, because u^* also decreases, the ratio remains nearly constant.

Molecular diffusion is an important factor to take into account in the interpretation of the measured entrainment rates when the Péclet number is small. Crapper & Linden (1974) suggested that the molecular-flux contribution is of importance when $P < 200$. Our experimental results tend to agree with Crapper & Linden's observations: when $P = 75$ ($Ri^* = 69$) the flux through most of the interfacial layer is predominantly by molecular diffusion, whereas when $P = 160$ ($Ri^* = 20$) the molecular flux contributes only moderately (figure 13).† Although it is of interest to have a good understanding of how and when molecular effects contribute to mixing across a density interface, application of the results to oceanic and atmospheric conditions is limited. There, the Péclet number is generally large due to the large scales involved. We therefore made an attempt to correct the entrainment rate by subtracting out the molecular contribution.

The correction is based on vertical flux profiles of the type shown in figure 13, which were measured at two downstream positions. From these profiles the rate of change of potential energy, in the layer δ, due to molecular flux and due to the total flux was calculated. The difference gives the turbulent part only.

† Our results are in close agreement with Crapper & Linden's results because the interfacial-layer thickness is of the order of the integral scale as in their experiments. In situations where $h < l$, we believe that molecular diffusion is of importance at $P > 200$ (if P is still defined with the scale l), because for a given turbulence the molecular-flux contribution depends on the interfacial gradient.

The ratio of the rate of change of potential energy due to the turbulent flux to that of the total flux is the weighting factor we applied to correct the entrainment velocity. It may be fortuitous, but in any case it is worth noting that the corrected entrainment velocity merges into the results of Kantha *et al.* (1977), which are taken as reliable at low values of Ri^*.

5.2. *Momentum balance*

As the boundary layer grows, a streamwise temperature gradient is set up which is positive in the mixed layer but negative along a horizontal which crosses the interface. The resulting effect is an adverse pressure gradient in the outer part of the boundary layer. For zero pressure gradient in the ambient flow the integral momentum equation gives

$$\left(\frac{u^*}{U_0}\right)^2 = \frac{d(m\delta)}{dx} - \frac{d}{dx}(\alpha\delta Ri_0), \tag{1}$$

where m is the ratio of momentum to boundary-layer thickness and α is a factor depending on the temperature defect. For a sharp interface $\alpha = \frac{1}{2}$, otherwise $\alpha < \frac{1}{2}$ (for a linear profile $\alpha = \frac{1}{3}$). The Richardson number Ri_0 is based on the ambient velocity U_0 and is defined by $Ri_0 = g(\Delta T/T)(\delta/U_0^2)$. Using $u_e = (d\delta/dx)U_0$ and assuming for the moment that m and α are independent of x, equation (1) gives an expression for the entrainment velocity in the form

$$\frac{u_e}{u^*} = \frac{Ri_0^{\frac{1}{2}} Ri^{*-\frac{1}{2}}}{m - \alpha Ri_0}. \tag{2}$$

It is seen from (2) that, for a power law $u_e/u^* \propto Ri^{*-\frac{1}{2}}$ to exist, it is necessary that Ri_0 be constant and that m and α be independent of Ri^*. In general, therefore, no simple power law in Ri^* should be observed. In the experiments reported here, Ri_0 also increases as Ri^* is increased (see table 1) and α and m are in fact weak functions of x (because the mean profiles do not remain similar) and also of Ri^* (see figure 5). The power-law behaviour is thus a very special case and may be observed only over a limited interval of Ri^* over which velocity and temperature profiles remain similar and Ri_0 does not change appreciably.

An interesting property of (2) is the singularity when $\alpha Ri_0 = m$. In order for the entrainment rate to remain finite, the boundary layer must separate ($u^*/U_0 \to 0$) when $\alpha Ri_0 \to m$. In the wind tunnel this would occur when $Ri_0 \simeq 0{\cdot}5$. The highest value obtainable in the tunnel used is 0·2, which is well below this critical value. It would be of interest to investigate separation due to entrainment in a larger tunnel. On the other hand, separation could of course be prevented by imposing a favourable pressure gradient on the ambient stream which would just compensate the adverse pressure gradient due to entrainment.

6. Conclusions and final remarks

Some interesting and useful conclusions result from this study. Firstly, there are indications that the interface acts in some respects as a solid boundary moving at U_0. The boundary effect increases with increasing stability: this shows up in the more pronounced inflection in the velocity profile as Ri^* increases and also in the behaviour

of the longitudinal and vertical r.m.s. turbulent velocities. The r.m.s. vertical velocity falls off monotonically across the interfacial layer whereas the longitudinal r.m.s. velocity stays constant well into the interface and then drops off rapidly. At the higher Reynolds number an amplification in u' is observed similar to that which is found when turbulence approaches a wall (Hunt & Graham 1978) without mean shear. Secondly, the entrainment velocity normalized by the shear velocity does not follow a power law in Ri^*. Momentum balance indicates also a dependence on the mean-flow Richardson number and furthermore shows that a critical value of Ri_0 exists beyond which a spatially developing boundary layer with zero ambient pressure gradient would separate. Separation is likely to occur at $Ri_0 \simeq 0{\cdot}5$.

The interfacial thickness h is consistent with the criterion for marginal stability of the interfacial layer as was conjectured by Kantha *et al.* (1977). The measured values of a gradient Richardson number in the interface are about $\frac{1}{3}$. Using this value, the relative thickness $h/\delta = k^2/3Ri^*$. For a rough-wall plane Couette flow which can be taken as a good representation of the mean velocity profile at large Ri^*, the value of k is about 13 ($\Delta U/u^* \simeq \frac{1}{2}U_0/u^* \simeq 13$ when using the value given in §3.3). This leads to $h/\delta \simeq 1/12Ri_0$. Thus, in situations where separation can occur at $Ri_0 \simeq 0{\cdot}5$, the interfacial layer thickness would not fall below $h/\delta \simeq \frac{1}{6}$.

Shear production in the interface is of little importance in the present experimental conditions and it will always be weak in the absolute sense due to the marginally stable state of the interfacial layer. At high stabilities its relative importance may, however, increase.

Time-lag correlations just above the centre of the interfacial layer show a behaviour characteristic of internal waves, namely that w has a 90° phase shift with respect to θ and u. These waves seem to occur as short wave packets. Their frequency corresponds closely to the buoyancy frequency of a turbulent eddy impinging on the interface. This indicates that the waves are predominantly horizontally propagating interfacial waves.

We are grateful to Professor G. M. Corcos for encouraging this work during the initial stages and to M. Caperan for some data processing. We especially want to thank Professor F. K. Browand for valuable comments on the final version of the paper. The work was partially financed by the Institut National d'Astronomie et de Géophysique under contracts ATP 3621 and ATP 3667.

REFERENCES

ARMI, L. 1977 Effects of density stratification on turbulence. *WHOI Summer Program*, p. 65, ref. no. 77–64.

ARYA, S. P. S. 1975 Buoyancy effects in a horizontal flat-plate boundary layer. *J. Fluid Mech.* **68**, 321–343.

CRAPPER, P. F. & LINDEN, P. F. 1974 The structure of turbulent density interfaces. *J. Fluid Mech.* **65**, 45–63.

GARTRELL, G. 1979 Studies on the mixing in a density-stratified shear flow. Ph.D. thesis, California Institute of Technology.

HINZE, J. O. 1975 *Turbulence*. McGraw-Hill.

HOPFINGER, E. J. 1973 Development of a stratified turbulent, shear flow. In *Proc Int. Symp. Stratified Flows, Novosibirsk*, 1972. A.S.C.E. Publication.

HOPFINGER, E. J. & TOLY, J. A. 1976 Spatially decaying turbulence and its relation to mixing across density interfaces. *J. Fluid Mech.* **78**, 155–175.

HUNT, J. C. R. & GRAHAM, J. M. R. 1978 Free-stream turbulence near plane boundaries. *J. Fluid Mech.* **84**, 209–235.

KANTHA, L. H., PHILLIPS, O. M. & AZAD, R. S. 1977 On turbulent entrainment at a stable density interface. *J. Fluid Mech.* **79**, 753–768.

KATO, H. & PHILLIPS, O. M. 1969 On the penetration of a turbulent layer into a stratified fluid. *J. Fluid Mech.* **37**, 643–655.

KOOP, C. G. & BROWAND, F. K. 1979 Instability and turbulence in a stratified fluid with shear. *J. Fluid Mech.* **93**, 135–159.

LINDEN, P. F. 1973 The interaction of a vortex ring with a sharp density interface: a model for turbulent entrainment. *J. Fluid Mech.* **60**, 467–480.

LINDEN, P. F. 1975 The deepening of a mixed layer in a stratified fluid. *J. Fluid Mech.* **71**, 385–405.

LOFQUIST, K. 1960 Flow and stress near an interface between stratified liquids. *Phys. Fluids* **3**, 158–175.

MCDOUGALL, T. J. 1979 Measurements of turbulence in a zero-mean-shear mixed layer. *J. Fluid Mech.* **94**, 409–431.

NICHOLL, C. I. H. 1970 Some dynamical effects of heat on a turbulent boundary layer. *J. Fluid Mech.* **40**, 361–384.

NIILER, P. P. & KRAUS, E. B. 1977 One dimensional models of the upper ocean. In *Modelling and Prediction of the Upper Layers of the Ocean* (ed. E. B. Kraus). Pergamon.

PHILLIPS, O. M. 1966 *The Dynamics of the Upper Ocean.* Cambridge University Press.

PIAT, J.-F. 1979 Pénétration d'une couche limite turbulente dans une interface de densité. Thèse de Docteur-Ingénieur, Université de Grenoble.

PRICE, J. F. 1979 On the scaling of stress-driven entrainment experiments. *J. Fluid Mech.* **90**, 509–529.

ROBERTSON, J. M. & JOHNSON, H. F. 1970 Turbulence structure in plane Couette flow. *Proc. A.S.C.E.* **96** (EM6), 1171–1182.

SCHLICHTING, H. 1960 *Boundary Layer Theory*, 4th edn. McGraw-Hill.

SCHON, J. P. & BAILLE, A. 1972 Méthode d' isolement des fluctuations turbulentes cinématiques et thermiques au moyen d'une sonde anémométrique à trois fils. *C.r. Acad. Sci. Paris* **274**, 116–000.

THOMAS, N. H. & HANCOCK, P. E. 1977 Grid turbulence near a moving wall. *J. Fluid Mech.* **82**, 481–486.

TURNER, J. S. 1968 The influence of molecular diffusivity on turbulent entrainment across a density interface. *J. Fluid Mech.* **33**, 639–656.

UZKAN, T. & REYNOLDS, W. C. 1967 A shear-free turbulent boundary layer. *J. Fluid Mech.* **28**, 803–821.